JOURNAL OF THEORETICAL AND APPLIED MECHANICS
63, 1, pp. 197-209, Warsaw 2025
https://doi.org/10.15632/jtam-pl/195836

EXPLORATION OF FREQUENCY CHARACTERISTICS OF BALL BEARING WITH UNEVEN LOAD BEARING EFFECT CAUSED BY WEAR FAILURE OF MULTIPLE ROLLING BODIES UNDER STARVED LUBRICATION

Zhong-Tang Huo, Jian-Qi Chen, Ling-Juan Hao, Jian-Song Gao
Handan University, Mechanical and Electrical College, Handan, China
corresponding author Zhong-Tang Huo, e-mail: huozhongtang123@hdc.edu.cn

Pointed at the problem of increased wear of rolling bodies (RBs) in a bearing under starved lubrication as well as abnormal vibration and increased noise of the bearing after occurence of wear fault, a fault dynamics model was proposed to simulate the interaction between components by quantifying the degree of rolling bodies wear. The results indicated that the bearing exhibited an uneven load bearing effect after the wear fault. The fractional multiple of the rotation frequency of the cage could be used as the basis for monitoring wear fault of rolling bodies. The research provides a reference for the diagnosis of wear fault in rolling bodies.

Keywords: starved lubrication, dynamic model, wear, bearing, frequency

1. Introduction

Ball bearings play an important role in modern industrial fields and are also a key link in the health monitoring and diagnosis of mechanical systems. The importance of their health status to the entire system cannot be ignored (Cao *et al.*, 2019; Visnadi and de Castro, 2019). Lubrication is an important factor affecting the performance of ball bearings during operation. In many cases, such as deterioration or reduction of the lubricant caused by extreme working conditions such as aircraft engines, the lubrication state of the bearing will transition to starved lubrication. The contact roughness between RBs and raceways will increase, and friction between internal components of will increase, thereby accelerating bearing wear. The levels of vibration and noise of the system are greatly grown, shortening the service life of the equipment (Wang *et al.*, 2018; Wen *et al.*, 2023). Therefore, for ensuring healthy and stable operation of the system, it is crucial to obtain accurate wear characteristics of RBs for the bearing condition monitoring.

The dynamic model is an important method to obtain various fault characteristics of bearings, it clarifies the fault mechanism, and establishes the mapping relationship between the fault excitation and characteristic frequency. Jiang *et al.* (2019) explored vibration mutation caused by contact force changes, Bai *et al.* (2021) explored the trend of outer ring fault frequency changes using temperature field thermal deformation theory, and for the study of RB fault, Zhang *et al.* (2021) established a dynamic model of the outer ring – RB composite faults to obtain fault characteristics. Cheng *et al.* (2019) set a local defect on the surface of RB and obtained the relationship between the geometric shape of the defect and deformation, the occurrence of local defect on RB significantly increased vibration of the bearing system. However, a wear fault cannot directly trigger impact forces like surface defects, so the local fault dynamics modeling method cannot be directly applied, but should be studied based on changes in size or spherical roundness. The above research clearly has low applicability. In addition, when conducting research on bearing dynamics, in order to reduce computational complexity, the bearings are generally considered to be in dry friction or a fully lubricated state (Liu *et al.*, 2020).

However, in actual use of bearings, it is almost impossible to achieve ideal lubrication conditions, and due to the influence of extreme working conditions, most bearings are in a state of starved lubrication (Maruyama and Saitoh, 2015). Bian *et al.* (2021) considered the influence of insufficient lubrication conditions on the bearing performance, and showed that when the lubricant oil supply was insufficient, the bearing was in the starved lubrication state, and the bearing bearing capacity of the oil film was reduced, which easily led to bearing wear. Regarding friction and wear behavior of RBs, Shi *et al.* (2022) developed a friction dynamics analysis model, which can be used to evaluate the lubrication and wear status of bearings, becoming the theoretical basis for establishing a friction lubrication model in this paper. Tu (2021) developed a dynamic model for sliding of cylindrical roller bearings. The most direct consequence of RB wear is a decrease in ball diameter. Regarding the difference in ball diameter, Bai *et al.* (2019) established a dynamic model suitable for full ceramic ball bearing considering RB size errors. Shi and Bai (2020) pointed out that the non-uniform loading situation varies with the diameter tolerance and arrangement of the RB, and the characteristic frequency of the RB raceway contact shifts from f_c to f_c', $2f_c'$ and $3f_c'$. By relying on the idea of ball diameter difference, this paper evaluates the phenomenon of uniform wear of RBs, and provides valuable materials for the study of dynamic models of RB wear.

From the above analysis, it can be seen that it is necessary to establish a dynamic model with RBs wear fault considering starved lubrication and obtain the corresponding vibration response of the fault. Therefore, the difference in ball diameter to simulate RBs wear fault was used in this paper, and based on the theory of friction-lubrication, the frequency characteristics of RBs wear fault under starved lubrication was obtained. The research results provide a sufficient reference for bearing wear fault monitoring in practical situations.

2. Establishment of the dynamic model for RB wear fault under starved lubrication

As shown in Fig. 1, $O_iY_iZ_i$ represents the center of mass coordinate system of the inner ring, and $O_jY_jZ_j$ represents the center of mass coordinate system of the j-th RB. The RB revolves around the outer ring axis at an angular velocity of ω_{mj}, while the cage rotates around the outer ring axis at ω_c. ϕ_j is the azimuth angle of the j-th RB in the coordinate system $O_iY_iZ_i$, and ψ_j is the azimuth angle of the j-th RB in the coordinate system OYZ.

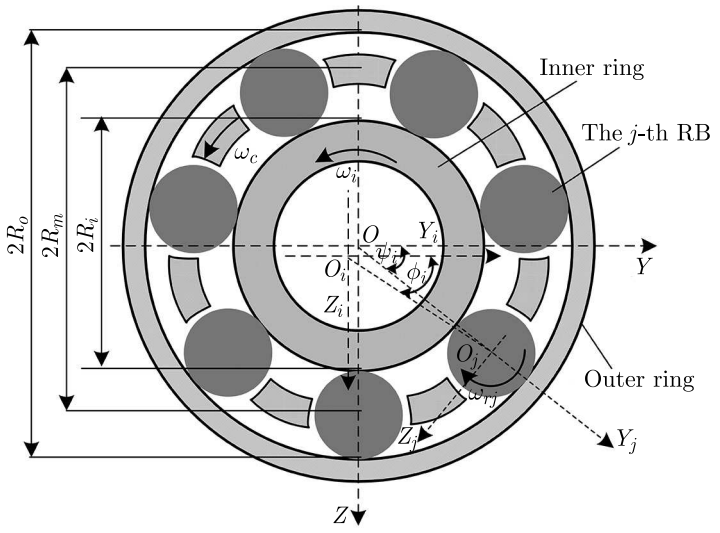

Fig. 1. Schematic of the rolling bearing

The azimuth ψ_j of the j-th RB can be expressed as

$$\psi_j = \omega_{mj} t + \theta_j + \frac{2\pi(j-1)}{N_b} \tag{2.1}$$

The diameter of the RB decreases after wear, and its load-bearing performance changes. D_j is the diameter of the RB, therefore, the relationship between ϕ_j and ψ_j is

$$\psi_j = \varphi_j + \arccos \frac{R_o^2 + R_i^2 - D_j(R_o - R_i) + 0.5D_j^2 - e^2}{2R_oR_i + D_j(R_o - R_i) - 0.5D_j^2} \tag{2.2}$$

where e is the eccentricity.

The deformation and force relationship between the RB and the raceway are as follows

$$\delta_j = \left[y\cos\varphi_j + z\sin\varphi_j - \frac{1}{2}\lambda - (D_j - D_b) \right]_+ \tag{2.3}$$

where "+" indicates that the equation takes only positive values. The contact force can be expressed as

$$Q_{ij} = K\beta\sqrt{\delta_j^3} \qquad Q_{oj} = K\beta\sqrt{\delta_j^3} + m_r R_m \omega_{mj}^2 \tag{2.4}$$

where K is the equivalent contact stiffness (Wang *et al.*, 2022); β is the switching function, it takes 1 when $\delta_j \geqslant 0$, otherwise it is 0.

Set the bearing area to cover the lower 1/3 symmetrical part of the bearing, as shown in Fig. 2. Due to wear on the RB, there is a difference between the actual ball diameter and the nominal diameter of the RB. Therefore, when the RB comes into contact with both the inner and outer rings, it is considered a load-bearing RB.

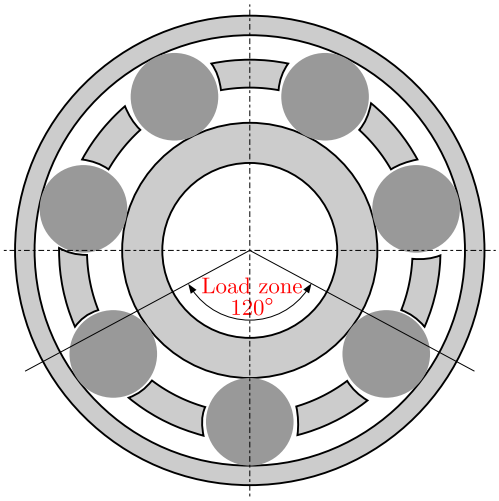

Fig. 2. Schematic of the bearing bearing area

When there is wear on the RB, that is, when there is a difference in the ball diameter of the RB, the ball diameter of the RB satisfies

$$D_j = D_n + A_j\delta \tag{2.5}$$

where A_j is the diameter coefficient corresponding to the j-th RB, and δ is the amplitude of the diameter difference.

When the j-th RB passes through the bearing area and D_{jlim} is given, the critical value for determining whether the RB is loaded can be obtained

$$D_{j\,\mathrm{lim}} = \frac{e^2 + R_o^2 - R_i^2 - 2eR_o(\psi_j - \psi_e)}{R_o + R_i - e(\psi_j - \psi_e)} \tag{2.6}$$

where ψ_e is the eccentricity angle of the inner ring, when $D_j \geqslant D_{j\,\mathrm{lim}}$, the j-th RB bears the load.

2.1. The traction force between RB and raceway under starved lubrication

When the RB and raceway are in the starved condition, due to the existence of micro-asperity contact friction between the two surfaces, the force relationship between the two contact surfaces will be affected, and one will need to calculate the oil film thickness and traction force under the starved condition, as shown in Fig. 3.

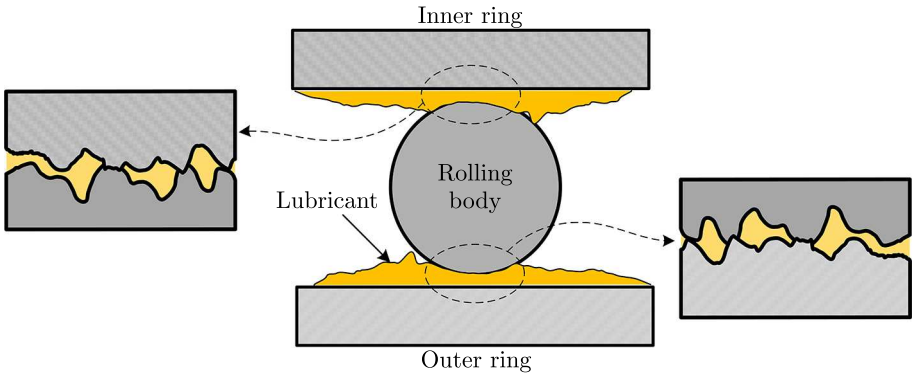

Fig. 3. Schematic of the contact surface between the RB and the raceway

The oil film thickness and traction force under the starved condition are calculated as

$$\begin{aligned} h_c = {} & 3.672R_y W^{-0.045\kappa^{0.18}} U^{0.663\kappa^{0.025}} G^{0.502\kappa^{0.064}} \\ & \cdot (1 + 0.025\overline{\sigma}^{1.248} V^{0.119} W^{-0.133} U^{-0.884} G^{-0.977} \kappa^{0.081})(1 - 0.573e^{-0.74\kappa}) \end{aligned} \tag{2.7}$$

and

$$(h_c)_{starved} = (1 - 1.561\chi^{0.849}\kappa^{-0.214})h_c \qquad \chi = 1 - \frac{\dot{m}_s}{\dot{m}_f} \tag{2.8}$$

where h_c is the film thickness in fully EHL, $(h_c)_{starved}$ is the film thickness in the state of starved lubrication, W is the dimensionless load, U is the dimensionless speed, G is the dimensionless material number, and V denotes the dimensionless hardness number, κ is the ellipticity coefficient, χ denotes the degree of starvation, $\dot{m}_s$ and $\dot{m}_f$ is the lubricant mass flow rate under starved conditions and fully EHL conditions, respectively.

The asperity contact ratio $L_{a-starved}$ of the micro-convex body between the RB and the raceway is calculated as

$$L_{a-starved} = 10W^{-0.083}U^{0.143}G^{0.314}\ln\left(1 + (1-\chi)^{-7.326}\overline{\sigma}^{4.689}V^{0.509}W^{-0.501}U^{-2.9}G^{-2.87}\right) \tag{2.9}$$

After quantifying the asperity contact ratio, the pressure distribution between the RB-raceway can be further determined

$$P_a = P_{max}\frac{L_{a-starved}}{100} \qquad P_h = P_{max}\left(1 - \frac{L_{a-starved}}{100}\right) \tag{2.10}$$

where P_{max} is the maximum contact pressure between the RB and the raceway contact surface, P_a is the contact pressure borne by the micro-asperity body, P_h is the contact pressure borne by the oil film.

Therefore, the traction force between the RB and the raceway can be calculated as

$$\begin{aligned} \tau(x', y') &= \min\Big[\frac{\eta(x', y')\Delta V}{(h_c)_{starved'}}, \Lambda P_h\Big] + f_c P_a \\ F_{i/oj} &= \iint \tau(x', y')\, dx'\, dy' \end{aligned} \tag{2.11}$$

where $\tau(x', y')$ is the oil film shear stress, $\eta(x', y')$ is the lubricant viscosity, ΔV is the sliding velocity between the RB and the raceway, Λ is the ultimate shear stress coefficient, and f_c denotes the roughness friction coefficient.

2.1.1. Establishment of bearing motion model

According to the Hertz theory and the geometric model of the bearing in Fig. 1, motion of the inner ring can be described as

$$\begin{aligned} W_y - \sum_{i=1}^{N_b}(Q_{ij}\cos\varphi_j - F_{ij}\sin\varphi_j) - m_i\frac{d^2y}{dt^2} &= c\frac{dy}{dt} \\ W_z - \sum_{i=1}^{N_b}(Q_{ij}\sin\varphi_j + F_{ij}\cos\varphi_j) - m_i\frac{d^2z}{dt^2} &= c\frac{dz}{dt} \end{aligned} \tag{2.12}$$

where c is damping.

Motion of the RB can be described as

$$\begin{aligned} F_{ij} - F_{oj} - Q_{cj} - m_r g\cos\psi_j - m_r R_m\frac{d\omega_{mj}}{dt} &= 0 \\ (F_{ij} + F_{oj})R_r - m_r R_m\omega_{mj}^2 R_r - m_r R_r^2\frac{d\omega_{rj}}{dt} &= 0 \end{aligned} \tag{2.13}$$

where ω_{mj} is the circumferential angular velocity of the j-th RB

$$\omega_{mj} = \frac{d\varphi_j}{dt} \tag{2.14}$$

Motion of the cage can be described as

$$R_m\sum_{i=1}^{N_b} Q_{cj} - J_c\frac{d\omega_c}{dt} = 0 \tag{2.15}$$

where J_c is the moment of inertia of the cage.

3. Numerical simulation

The 6304 deep groove ball bearing is taken as an example for the study, and the parameters of the bearing and the performance parameters of the lubricant are shown in Table 1. The operating temperature is 40°C, radial load $W = 100$ N, inner ring speed $\omega_i = 4000$ r/min.

When the bearing area is uniformly loaded, the number of loaded RBs $N = N_b/3$, and the number of RBs in the bearing studied in this paper is $N_b = 7$. Based on Fig. 2, it can be seen that the number of loaded RBs in the bearing area varies between 2 and 3 without considering the difference in ball diameter. This paper introduces wear in three RBs, assuming the radii of

Table 1. Main parameters of rolling bearing

Parameters	Value	Parameters	Value
Outer raceway radius R_o [mm]	22.77	Raceway surface roughness σ_1 [μm]	0.028
Inner raceway radius R_i [mm]	13.24	Surface roughness of ball σ_2 [μm]	0.042
Bearing pitch circle radius R_m [mm]	18	Material cypress pine ratio v	0.3
RB radius R_r [mm]	4.76	Density of lubricant ρ [Kg/m^3]	826
Number of RBs N_b	7	Lubricant in viscosity η_0 [Pa·s]	0.04
Radial clearance ε [mm]	10e-5	Ultimate shear stress coefficient Λ	0.0434

the three worn RBs are 4.71 mm, 4.71 mm and 4.70 mm, respectively. The analysis of the sliding effect and force is based on the worn RB. Using a fixed time step ($\Delta t = 5 \cdot 1\text{e-}4$), the fourth-order Runge-Kutta algorithm in Matlab is incorporated to solve differential equation systems.

The above analysis indicates that there may be 1-3 load-bearing RBs in the bearing area, as shown in Fig. 4. Figure 4 shows the situation of different numbers of load-bearing RBs or worn RBs in the bearing area, where the worn RBs are represented by dashed lines. The solid line represents healthy RBs.

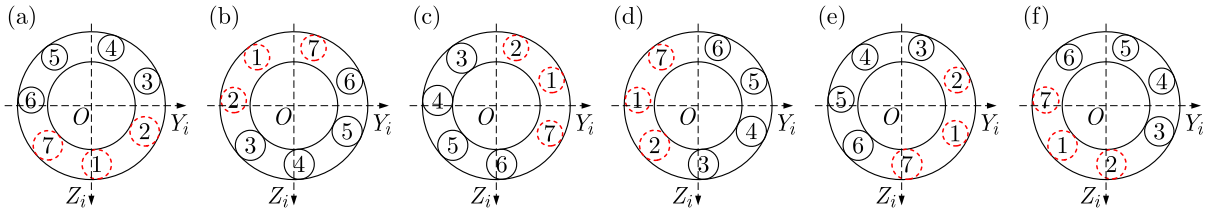

Fig. 4. Different bearing conditions

Numerical simulation methods are used to solve the model, as shown in Fig. 5. In Fig. 5a, the RB enters the contact zone when the azimuth angle is around $\phi_j = 300°$, and it can be observed that the oil film thickness between the RB and the raceway decreases with an increase of the starved lubrication degree. The reason for this phenomenon is that the supply of the lubricant is insufficient, and the rotating pair cannot stimulate enough lubricant to form an oil film. In the load area, due to the effect of gravity and load, the oil film is compressed, and thickness of the oil film is much lower than that in the non loaded area.

An increase in the degree of starved lubrication leads to an increase in friction between the RB-raceway, which drives the RB to rotate around the center of the bearing at an increased rate, i.e., the rotational speed of the RB and cage increases with the increase in the degree of starved lubrication, as shown in Figs. 5b and 5c. In Fig. 5b, the dashed line represents the rotational speed of the RB experiencing wear failure, which is lower than the healthy RB under the same lubrication conditions. Figure 5d shows the RB-raceway slip velocity, in the contact zone the RB is subjected to the radial load, so the slip velocity decreases rapidly. In addition it can be clearly observed that the slip rate decreases rapidly with an increase of the starved degree within one week of RB rotation.

Figure 6a shows the contact forces between the RBs and the raceway of the ball bearing without considering wear of the RBs, and the contact forces of each RB in the load zone are almost equal. Figures 6b-6d show the bearing capacity of each RB under the initial condition $\chi = 0$. Figure 6b corresponds to Fig. 4a, where the contact force of RBs 1, 2 and 7 is significantly lower than that of other RBs, exhibiting a significant uneven bearing effect. The 6th and 3rd RBs adjacent to the 7th and 2nd RBs have the highest contact force. This is because the diameter of the 1st, 2nd and 7th RBs is small, and according to the Hertz theory, the Hertz force generated is small. Therefore, the contact force is distributed to the 6th and 3rd RBs. Figures 6c and 6d are consistent with this description principle, where the RB with smaller diameter bears less

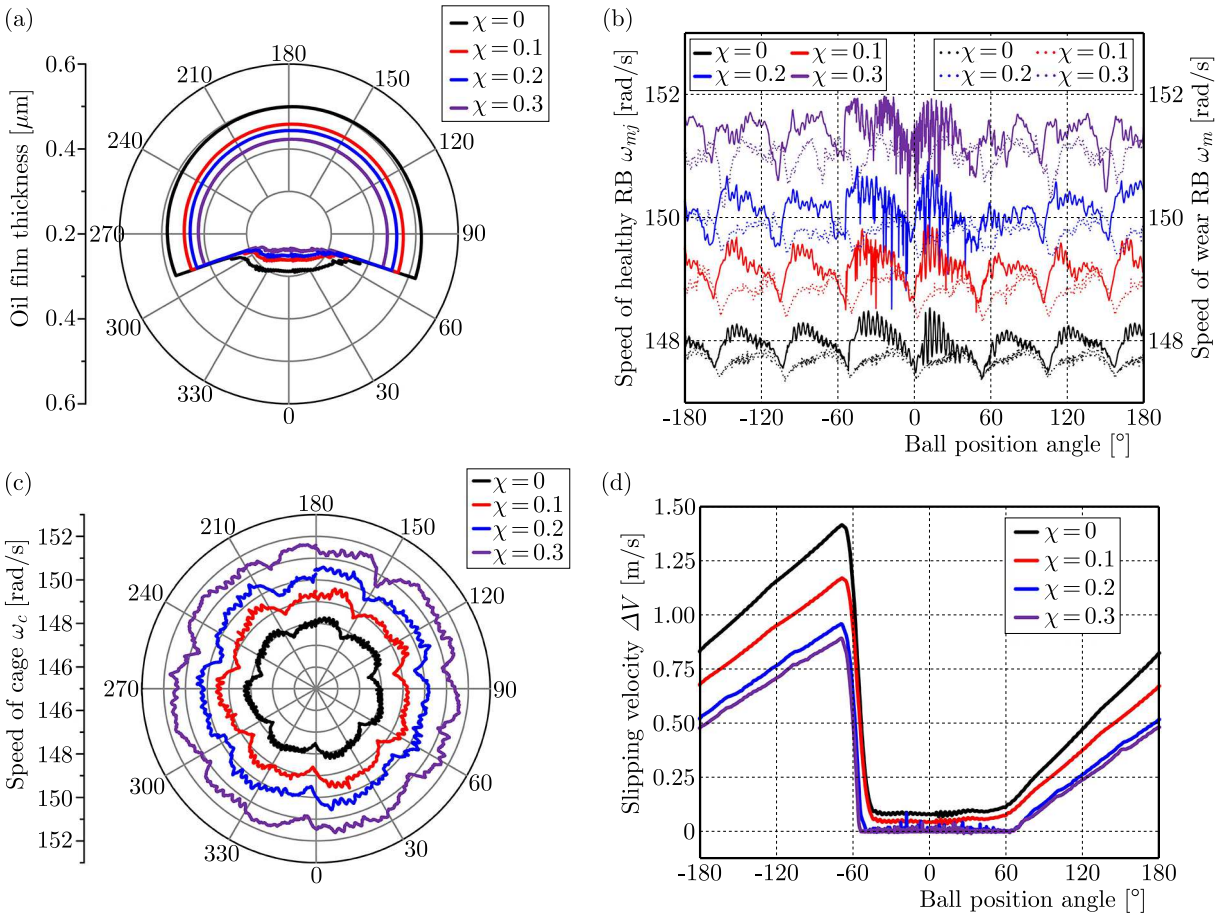

Fig. 5. Related calculation results: (a) the influence of starved lubrication on oil film thickness, (b) revolution speed of RB, (c) cage speed, (d) sliding speed of RB to raceway

pressure, while the adjacent RBs have a greater contact force, resulting in a significant uneven bearing effect.

Figure 7 shows variation of rhe contact force between each RB and the raceway at different χ values of 0, 0.1, 0.2 and 0.3. Figure 7 more intuitively reflects that the contact force of RBs 1, 2 and 7 is significantly lower than the others. And the 1st RB is adjacent to both the 7th and 2nd RBs, so a portion of the contact force from the 7th and 2nd RBs is shared on the 1st RB. In addition, as the degree of starved lubrication increases, the thickness of the oil film inside the bearing decreases, the contact stiffness K increases, resulting in an overall upward trend in the contact force (Wang *et al.*, 2022).

Equation (3.1) provides the calculation method for the friction torque between the RB and the raceway. Figure 8 shows variation of the friction torque for different degrees of starved lubrication. The curves A, B, C and D represent the depleted oil conditions at $\chi = 0$, 0.1, 0.2 and 0.3, respectively. After the wear of the RBs, as the degree of starved lubrication increases, the friction torque increases. In addition, changes in the friction torque can affect the degree of bearing sliding. According to Tu *et al.* (2021), the more sufficient friction between the RB and the raceway, the greater the driving force provided for the RB and the cage, thereby suppressing bearing sliding. With an increase of χ, that is an increase of the friction torque, the slip effect is reduced, verifying a decrease in slip velocity, which is consistent with Tu's research results. Meanwhile, this also confirms the conclusion in Fig. 5 that the sliding effect is suppressed as the degree of starved lubrication increases after the wear of the RB

$$M_{f,average} = \text{AVERAGE}\left[\sum_{j=1}^{N_b}(F_j R_j + F_o R_o)\right] \tag{3.1}$$

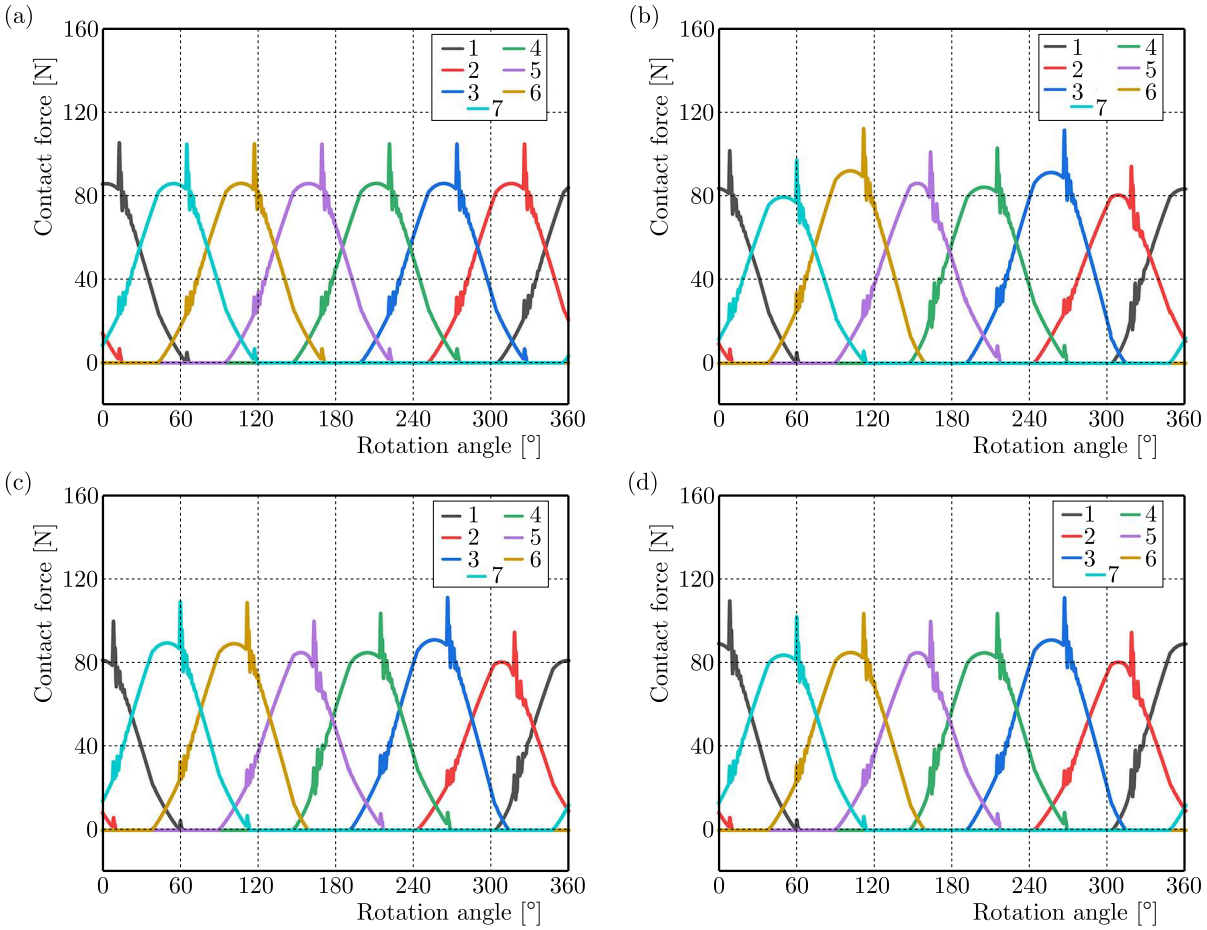

Fig. 6. The bearing capacity of each RB under the initial lubrication state

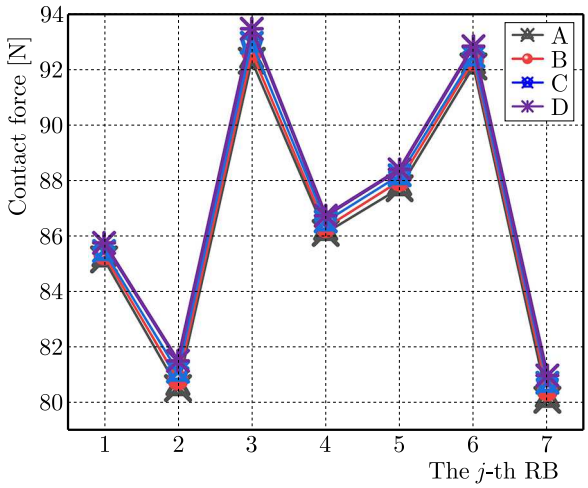

Fig. 7. The bearing capacity of each RB under different degrees of starved lubrication

The spectrum of Fig. 9 was obtained by solving the differential equation. Nf_r is the rotational frequency, where $nf_{cA,B,C,D}$ correspond to the rotational frequency and doubling frequency of the cage under four lubrication states, while $f_{bwA,B,C,D}$ correspond to the characteristic frequencies of RB wear faults. According to Shi's research (Shi *et al.*, 2019), when uneven load bearing effects occur inside the bearing, a fractional multiple of the cage frequency f_c, $f_{cw} = 3f_c/N$, appears in the spectrum. The above formula provides the characteristic frequency when there is

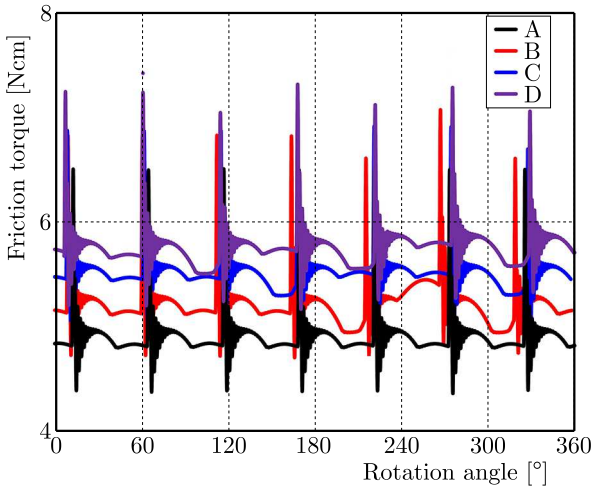

Fig. 8. Friction torque between the RB and raceways under different degrees of starved lubrication

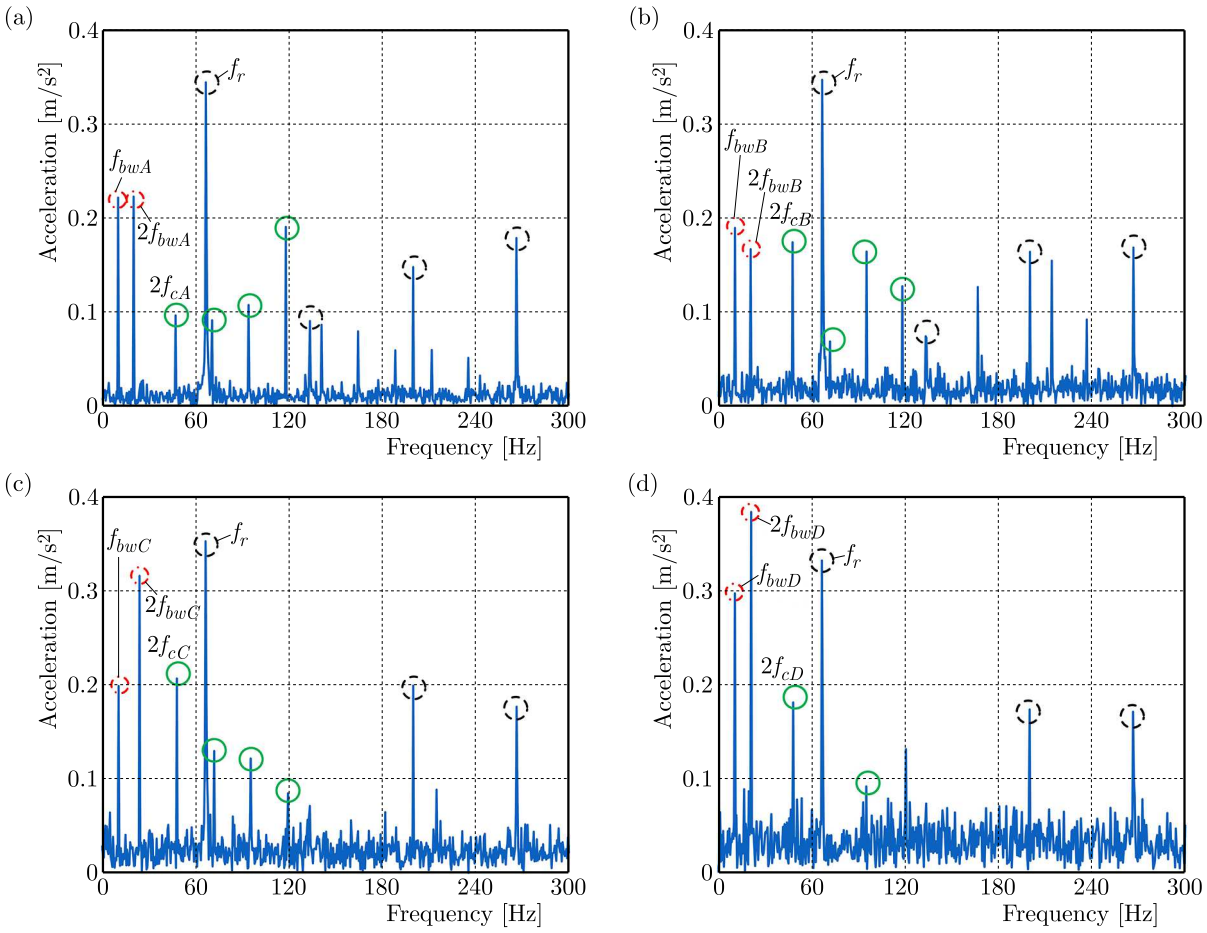

Fig. 9. Vibration spectrum of bearing dynamics model simulation: (a) A, (b) B, (c) C, (d) D

only one loaded RB in the bearing area, and when there is $2, 3, \ldots, N/3$ in the bearing area, the corresponding characteristic frequencies are $2f_{cw}, 3f_{cw}, \ldots, Nf_{cw/3}$. For the bearings selected in this article, there are 7 RBs, and there may be 1,2,3 loaded RBs simultaneously in the bearing area. When the worn RBs enter the bearing area, there are 2 loaded RBs in that area, and the corresponding characteristic frequency in the spectrum is $2f_{cw}$. After the worn RB leaves the

bearing area, there are three loaded RBs in that area. At this time, $3f_{cw} > f_c$, and the load-bearing characteristics of bearings after RB wear will appear as f_c and its harmonic components.

As the degree of starved lubrication, the friction torque between the RB and the raceway increases, and the sliding effect is suppressed. This is manifested by an increase in the rotational frequency f_c and its harmonic component nf_c of the cage, but still lower than the theoretical value in ideal conditions. The spectrum shows an increase in f_{cA}, f_{cB}, f_{cC} and f_{cD}, corresponding to an increase in the RB wear frequency f_{bwA}, f_{bwB}, f_{bwC} and f_{bwD}, as shown in Fig. 9 and Table 2.

Table 2. Characteristic frequencies at different degrees of starved lubrication

Item	$\chi = 0$	$\chi = 0.1$	$\chi = 0.2$	$\chi = 0.3$	Change rate
f_c [Hz]	23.83	23.95	24.19	24.32	1.9%
f_{cw} [Hz]	20.19	20.38	20.80	20.92	3.5%

4. Experimental study

For verifying the correctness of the model proposed in this paper and detect the bearing vibration characteristics of RB wear fault under starved lubrication, an experimental setup as shown in Fig. 10 was established in this Section. In Fig. 10, the speed was controlled by a speed controller, and the motor output speed was from 0 to 5000 r/min. The vibration signal was obtained by a contact type acceleration sensor arranged on the bearing seat and further processed by a data collector, with a sampling frequency of 5000 Hz. The selected bearings were consistent with those in the simulation in the previous Section. Through special customization and procurement, the RB had a radius of 4.70 mm, the radius of the two RBs is 4.71, while the other RBs had the radius of 4.76 mm. This paper designed three sets of experiments P, Q and R. By manually adding or removing lubricants, the lubricants in the bearing cavity during the three sets of experiments were 0%, 33% and 75% of the cavity volume, respectively, to simulate changes in the degrees of starved lubrication.

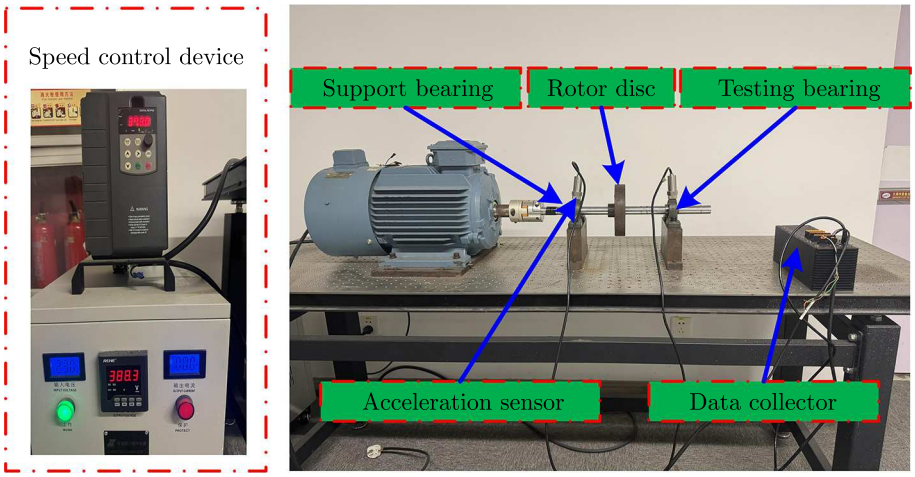

Fig. 10. Experimental testing system

Set the motor output speed to 4000 r/min, collect vibration data after the speed stabilizes, and perform Fourier transform on the vibration signal to obtain the spectrum of the right bearing as shown in Fig. 11. In the spectrum, it is clear to see changes in the characteristic frequencies $f_{cwP,Q,R}$ of RB wear caused by changes in lubricant supply, while the rotational frequency f_r and its harmonic components related to input speed remain unchanged. In the P, Q and R tests,

the corresponding RB wear characteristic frequencies were 10.02 Hz, 10.24 Hz and 10.78 Hz, respectively. The corresponding double wear characteristic frequencies are approximately in the range of 20 Hz-22 Hz, which is consistent with the simulation results. The corresponding cage rotation frequency and its harmonic components were also excited. However, due to frequency modulation and mutual influence, the amplitude of the first harmonic frequency $f_{cP,Q,R}$ of the cage rotation was relatively low, which may be submerged in background noise in practice. However, the RB wear characteristic frequencies still vary significantly.

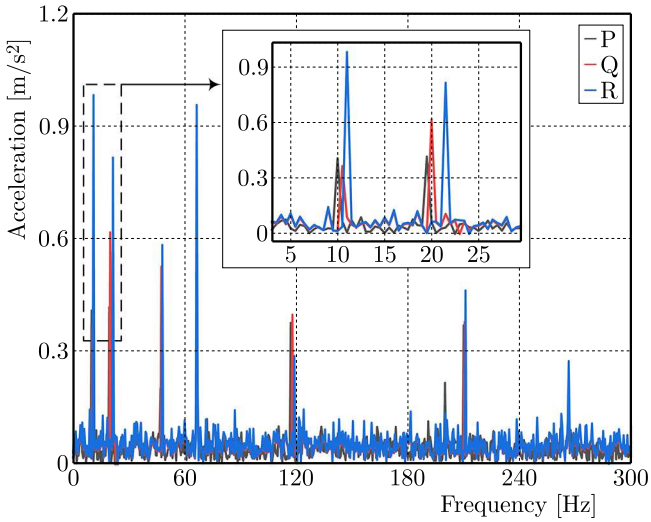

Fig. 11. Frequency curve of experimental data

Compared with simulation, it is difficult to accurately simulate the increase and decrease of lubricants. However, this experiment still verified the hypothesis that the characteristic frequency changed with the degrees of starved lubrication, and quantified the characteristics of RB wear fault under different degrees of starved lubrication, proving the correctness of the theoretical model and calculation.

5. Conclusion

This paper quantified the wear failure of ball bearings under starved lubrication based on the idea of ball diameter difference of RBs, and the mechanism of fault characteristics was analyzed by contact-friction theory. The main conclusions are as follows:

(1) RB wear failure is the cause of an uneven bearing load. Specifically, the contact force between the worn RB and the ring is small, while the adjacent healthy RBs experience a greater contact force.
(2) Deterioration of lubrication conditions will exacerbate the wear failure of RB. Specifically, as the degrees of starved lubrication increases, the same RB will experience greater contact and friction forces, leading to wear faults quickly radiating to healthy RBs.
(3) At the same lubrication level, the worn RB speed is slightly lower than healthy RBs. Specifically, due to wear of RB, it experiences a lower contact force and lower frictional driving force than healthy RB, resulting in a decrease in orbital speed.
(4) The fractional multiple of the rotation frequency of the cage can be used as an indicator for monitoring the RB wear fault. Specifically, considering the total number of RBs, the number of RBs loaded within the load zone, and the number of RBs experiencing wear and tear fault, relevant frequency components can be found in the spectrum.

(5) A change in the lubrication state will have an impact on the characteristic frequency of wear fault. In the actual monitoring of the ball bearing wear fault, lubrication conditions should be fully considered to effectively distinguish characteristic frequencies and ensure the accuracy of fault monitoring.

In the future, we will focus on the temperature rise phenomenon caused by bearing operation heating, fully consider the influence of temperature rise on lubrication conditions, radial clearance, and component dimensions, and incorporate the wear phenomenon of raceways into our research. We will establish a more detailed, comprehensive, and applicable bearing wear dynamic model to improve the theory of bearing fault dynamics.

References

1. Bai X.T., Wu Y.H., Rosca I.C., Zhang K., Shi H.T., 2019, Investigation on the effects of the ball diameter difference in the sound radiation of full ceramic bearings, *Journal of Sound and Vibration*, **450**, 231-250
2. Bai X., Zheng H., Wang Z., Wang Z., 2021, Raceway defect frequency deviation of full-ceramic ball bearing induced by fit clearance in wide temperature ranges, *Shock and Vibration*, **2021**, 1, 6650798
3. Bian Z., Song C., Meng L.H., Zhou Q.H., 2021, Response of the interface between the ball and the raceway of rolling bearing under starved lubrication, *IOP Conference Series: Materials Science and Engineering*, **1043**, 5, 052005
4. Cao H., Shi F., Li Y., Li B., Chen X., 2019, Vibration and stability analysis of rotor-bearing--pedestal system due to clearance fit, *Mechanical Systems and Signal Processing*, **133**, 106275
5. Cheng H., Zhang Y., Lu W., Yang Z., 2019, Research on ball bearing model based on local defects, *SN Applied Sciences*, **1**, 10, 1219-1229
6. Jiang Y., Huang W., Luo J., Wang W., 2019, An improved dynamic model of defective bearings considering the three-dimensional geometric relationship between the rolling element and defect area, *Mechanical Systems and Signal Processing*, **129**, 694-716
7. Liu Y., Wang W., Qing T., Zhang Y., Liang H., Zhang S., 2020, The effect of lubricant temperature on dynamic behavior in angular contact ball bearings, *Mechanism and Machine Theory*, **149**, 103832
8. Maruyama T., Saitoh T., 2015, Relationship between supplied oil flow rates and oil film thicknesses under starved elastohydrodynamic lubrication, *Lubricants*, **3**, 2, 365-380
9. Shi H.T., Bai X.T., 2020, Model-based uneven loading condition monitoring of full ceramic ball bearings in starved lubrication, *Mechanical Systems and Signal Processing*, **139**, 106583
10. Shi H.T., Bai X.T., Zhang K., Wu Y.H., Yue G.D., 2019, Influence of uneven loading condition on the sound radiation of starved lubricated full ceramic ball bearings, *Journal of Sound and Vibration*, **461**, 114910
11. Shi X., Lu X., Feng Y., Qiu Z., 2022, Tribo-dynamic analysis for aero ball bearing with 3D measured surface roughness, *Engineering Failure Analysis*, **131**, 105848
12. Tu W., Yu W., Shao Y., Yu Y., 2021, A nonlinear dynamic vibration model of cylindrical roller bearing considering skidding, *Nonlinear Dynamics*, **103**, 3, 2299-2313
13. Visnadi L.B., de Castro H.F., 2019, Influence of bearing clearance and oil temperature uncertainties on the stability threshold of cylindrical journal bearings, *Mechanism and Machine Theory*, **134**, 57-73
14. Wang Y., Yan C., Lu Z., Liu Y., Wu L., 2022, Effect of thermal elastohydrodynamic lubrication on vibration characteristics of ball bearing with local defect, *Proceedings of the Institution of Mechanical Engineers, Part K: Journal of Multi-Body Dynamics*, **236**, 3, 488-500

15. Wang Z., Yu Q., Shen X., Chen X., 2018, A simple model for scuffing risk evaluation of point contact under mixed lubrication, *Journal of Tribology*, **140**, 3, 031502

16. Wen C., Meng X., Gu J., Xiao L., Jiang S., Bi H., 2023, Starved lubrication analysis of angular contact ball bearing based on a multi-degree-of-freedom tribo-dynamic model, *Friction*, **11**, 8, 1395-1418

17. Wu X., Qin Y., Luo J., Wang S., Chen B., 2022, Fault dynamic model of high-speed rolling bearing by a compound displacement excitation function considering the effect of defect roughness, *Mechanism and Machine Theory*, **177**, 105061

18. Zhang X., Yan C., Liu Y., Yan P., Wang Y., Wu L., 2020, Dynamic modeling and analysis of rolling bearing with compound fault on raceway and rolling element, *Shock and Vibration*, **2020**, 1, 8861899

Manuscript received July 18, 2024; accepted for publication November 11, 2024